Stem Cell Reports
Article
OPEN ACCESS

Derivation of Traceable and Transplantable Photoreceptors from Mouse Embryonic Stem Cells

Sarah Decembrini,[1,*] Ute Koch,[2] Freddy Radtke,[2] Alexandre Moulin,[3] and Yvan Arsenijevic[1,*]
[1]Department of Ophthalmology, University of Lausanne, Jules-Gonin Eye Hospital, FAA, Unit of Gene Therapy & Stem Cell Biology, Avenue de France 15, 1004 Lausanne, Switzerland
[2]École Polytechnique Fédérale de Lausanne, Institut Suisse de Recherche Expérimentale sur le Cancer, 1015 Lausanne, Switzerland
[3]Department of Ophthalmology, University of Lausanne, Jules-Gonin Eye Hospital, FAA, Eye Pathology Laboratory, Avenue de France 15, 1004 Lausanne, Switzerland
*Correspondence: sarah.decembrini@fa2.ch (S.D.), yvan.arsenijevic@fa2.ch (Y.A.)
http://dx.doi.org/10.1016/j.stemcr.2014.04.010

SUMMARY

Retinal degenerative diseases resulting in the loss of photoreceptors are one of the major causes of blindness. Photoreceptor replacement therapy is a promising treatment because the transplantation of retina-derived photoreceptors can be applied now to different murine retinopathies to restore visual function. To have an unlimited source of photoreceptors, we derived a transgenic embryonic stem cell (ESC) line in which the *Crx*-GFP transgene is expressed in photoreceptors and assessed the capacity of a 3D culture protocol to produce integration-competent photoreceptors. This culture system allows the production of a large number of photoreceptors recapitulating the in vivo development. After transplantation, integrated cells showed the typical morphology of mature rods bearing external segments and ribbon synapses. We conclude that a 3D protocol coupled with ESCs provides a safe and renewable source of photoreceptors displaying a development and transplantation competence comparable to photoreceptors from age-matched retinas.

INTRODUCTION

Retinal degenerative diseases such as inherited or age-related eye diseases resulting in the loss of photoreceptors are the leading cause of blindness in Europe. To date, around 4% of the western world population suffers from one of these diseases, and unfortunately, no cures exist to treat the majority of them (Prokofyeva and Zrenner, 2012). Up to now, only gene therapy applied at the very early stage of the disease provides encouraging results by slowing down the degeneration progression (Bemelmans et al., 2006; Bainbridge et al., 2008; Maguire et al., 2008), but no data indicate that gene therapy with the present tools can in fact stop the degenerative process in patients (Cideciyan et al., 2013). Around 200 different mutated genes and loci were identified so far to be responsible for roughly half of the retinal dystrophy cases, revealing that a substantial number of patients necessitate alternative therapies. Interestingly, during retinal degeneration, the mammalian retina is unable to regenerate, but the underlying retinal circuitry is relatively well preserved for a long time. Different groups therefore validated the possibility to reactivate dormant retinal circuits of degenerating retinas, focusing on methods such as retinal prosthetic systems, optogenetic approaches, and cell replacement therapy (Busskamp and Roska, 2011; Mathieson et al., 2012; MacLaren et al., 2006). Restoring photosensitivity by transplanting new photoreceptors and coupling them to the remaining active retinal circuitry is thus a realistic approach. Photoreceptor cells collected directly from either newborn or adult donor retinas can be effectively transplanted into adult wild-type retinas and restore photosensitivity as well as some visual function in mouse models of retinal degeneration (MacLaren et al., 2006; West et al., 2009; Gust and Reh, 2011; Pearson et al., 2012; Singh et al., 2013). Because the developing retina is not a suitable renewable source of photoreceptors, many groups focused their attention on different stem cells due to their potential to provide an unlimited supply of the desired cell phenotype (Tomita et al., 2002; Klassen et al., 2004; Zhang et al., 2004; Cicero et al., 2009; Gualdoni et al., 2010; Decembrini et al., 2011). To date, the best cell sources identified to efficiently generate photoreceptors in vivo are the pluripotent embryonic stem cells (ESCs) and the induced pluripotent stem cells (iPSCs). Recently, many groups have developed protocols to induce the differentiation of photoreceptors from human or mouse ESCs (hESCs or mESCs, respectively) and iPSCs (Lamba et al., 2006, 2009, 2010; Osakada et al., 2008; Hirami et al., 2009; Meyer et al., 2009; Tucker et al., 2011; Nakano et al., 2012). However, few studies investigated the capacity of photoreceptors derived from ESCs and iPSCs to integrate the retina. Up to now, two different publications have shown the generation of human retinal cells from pluripotent cells that, after transplantation, migrate into the outer nuclear layer (ONL), acquiring a photoreceptor-like morphology and expressing some photoreceptor markers (Lamba et al., 2009; Tucker et al., 2011). Although encouraging, these works did not provide a characterization of the cell type or of the developmental stage amenable to produce

photoreceptors that integrate the recipient retina. Moreover, the lack of well-formed external segments and mature ribbon synapses precludes a firm conclusion of truly integrated photoreceptors. In addition, the use of viral vectors to label transplanted cells could have led to false-positive results (West et al., 2012). So far, only one study has described the attempt to produce enough mESC-derived photoreceptors for cell replacement therapy, concluding that the 2D culture system utilized cannot be scaled up to produce integration-competent photoreceptors (West et al., 2012). These results diverge with the 2D systems previously exploited with human cells (Lamba et al., 2009; Tucker et al., 2011). Recently, the group of Y. Sasai published a new 3D culture system (Eiraku et al., 2011; Eiraku and Sasai, 2012) to induce the formation of optic cups (OCs) generating retina-like tissues containing all the retinal cell types including photoreceptors. Importantly, such photosensitive cells were not challenged for their capacity to integrate a retina after transplantation. In this study, we derived transgenic mESC lines in which the reporter gene, the *Crx*-GFP transgene, is expressed in postmitotic photoreceptor cells. Taking advantage of such lines, we evaluated the extent to which the above-mentioned 3D culture system recapitulates photoreceptor genesis and in parallel assessed the capacity of in-vitro-generated photoreceptors to integrate recipient retinas in correlation with their stage of culture.

RESULTS

De Novo Isolation of a *Crx*-GFP ESC Line from Blastocysts

Within the last 2 years, the group of Y. Sasai (Japan) published two landmark papers describing a 3D culture system to generate synthetic OCs from mESCs and hESCs (Eiraku et al., 2011; Eiraku and Sasai, 2012). Such a culture system offers the unique opportunity to study mammal retinogenesis in vitro and to exploit the photoreceptor capacity to integrate the retina after grafting. In order to follow photoreceptor development and to trace cells after transplantation, we derived three ESC lines from a transgenic mouse line expressing GFP under the control of the endogenous photoreceptor-specific promoter *Crx* (Samson et al., 2009). At the onset of the mouse retinogenesis, the CRX protein is translated in developing photoreceptor precursors (from embryonic day 13 [E13]). In the adult murine retina, its expression is restricted to both mature cones and rods (Samson et al., 2009). For our ESC line, blastocysts were isolated from a *Crx*-GFP-positive female at 3.5 days postcoitum (dpc) as described by Bryja et al. (2006a, 2006b) with minor adjustments (Kiyonari et al., 2010; Wray et al., 2010, 2011) consisting with the addition of CHIR99021 and PD184352 molecules to block the glycogen synthase kinase 3 β and mitogen-activated protein (MEK) pathways, respectively, and increase ESC resistance to differentiation (Figures S1A–S1D available online). Clones positive for the pluripotency markers (Figures S1E–S1M) were tested for the teratoma assay. For each line, five adult nonobese diabetic (NOD)/severe combined immunodeficiency (SCID) mice were injected subcutaneously with 1×10^6 ESCs (see Supplemental Experimental Procedures). Three weeks postinjection, teratomas were sampled and analyzed by hematoxylin and eosin staining for the tissue composition. All the lines tested gave rise to a rapid teratoma outgrowth composed of a mixture of tissues derived from all three germinal sheets (Figures S1N–S1S).

Optimization of the OC and Photoreceptor Generation

Optic Vesicle and Cup Morphogenesis

Taking advantage of recently published milestone work by Eiraku et al. (2011) and Eiraku and Sasai (2012) describing the in vitro generation of OCs, we optimized and scaled up a 3D culture protocol to generate transplantation-competent photoreceptor cells from mESCs. Briefly, the five phases of the former protocol are day 0, which is a quick aggregation step to induce the formation of embryoid body (EB)-like structures; day 1, addition of basement-membrane matrix components to promote the development of a neuroepithelium around the EBs from which different optic vesicles (OVs) will be specified; day 7, EBs transfer into floating culture conditions to induce the OC formation (Figures 1A–1L); day 10, OC isolation; and day 13, switch medium to induce photoreceptor differentiation. In the following experiments, three different *Crx*-GFP ESC lines were used (clones 3, 6, and 8). We first assessed the ideal cell density to generate the highest number of photoreceptors by producing individual aggregates containing from 1,500 to 12,000 ESCs (15–120 cells/μl of medium). The optimal cell density, leading to a large production of photoreceptors, was found to be 3,000–5,000 cells per aggregate depending on the line used. A higher number of cells had no positive impact. A lower number of cells resulted in the failure of the neuroepithelium formation. In addition, after 25 days of culture, we observed that only OVs with a size superior to 300 μm between days 5 and 7 of culture (Figure 1M), and with a flattened distal portion by days 7–9 (Figures 1G, 1K, and 1L, black arrows), gave the highest number of photoreceptors. This OV population represents around 70% of the total retinas generated. Then, the increased time in Matrigel improved the OC formation from one out of five (20%) to one out of three (33%) initial OVs as well as the harvesting of retina-like structures (Figure 1N). Concerning the OC isolation (at day 10), we assessed the option of growing developing retinas directly inside the mother aggregate, instead

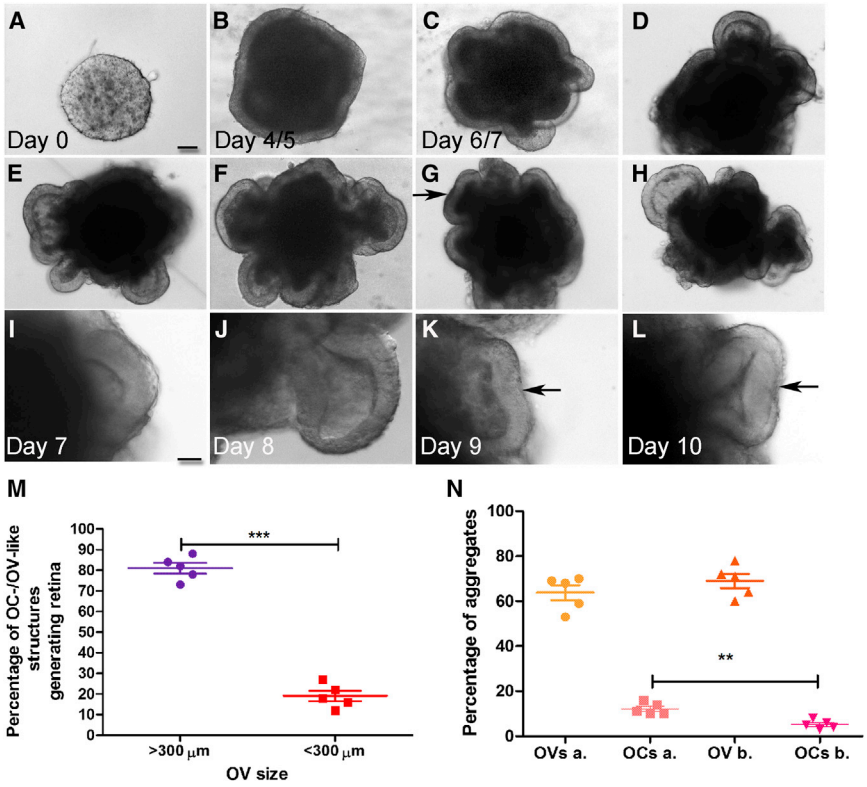

Figure 1. Time Course of OV and OC Formation from mESCs and Quantification

(A) Single aggregate formation in serum-free floating culture of EB-like aggregate with quick reaggregation conditions.

(B) Neuroepithelium formation.

(C–H) Different examples of OV evagination from specialized area of the neuroepithelium.

(I–L) Flattening of the OV distal portion and invagination. (G, K, and L) Examples are shown of OV flattened at varied differentiation days (black arrows).

(M) Quantification of the diameter of OV giving rise to retinas.

(N) Quantification of OC and OV generation before and after the protocol fine-tuning. Error bars, mean ± SEM (n = 7 independent experiments with 96 cells counted per experiment). **p < 0.01 and ***p < 0.001, by t test. a, after; b, before. Scale bars, 150 μm (A) and 100 μm (I).

of dissecting them as previously described by Eiraku et al. (2011). In fact, the deletion of tissue adjacent to the OC provoked unpredictable consequences likely due to its potential role in retina patterning and differentiation.

Boosting the Photoreceptor Differentiation

In order to improve and scale up the photoreceptor production, we fine-tuned the 3D culture system by adding ingredients and adjusting the dioxygen (O_2) concentration. The use of supplements such as N2 and B27 (see Supplemental Experimental Procedures) instead of the original mix of retinoic acid (RA), N2, and 10% of fetal calf serum (FCS) produced a series of benefits. Indeed, we observed that the absence of serum reduces the growth of nonneural tissues and that the B27 supplement favors neuroectoderm development. In addition we exploited the consequences of a different O_2 concentration on aggregates at different days of culture. Age-matched aggregates (day 7 or day 12) were placed in floating conditions to induce retina maturation and incubated at either atmospheric O_2 concentration or in hyperoxia. Aggregates from day 7 culture incubated at 40% of O_2 exhibited increased apoptosis up to day 12 with a sequential reduction of the OV-OC dimension: for clone 3.48% ± 1.3% of the GFP-positive structures showed a reduced size and 39% ± 2.4% for clone 6 (data not shown). Conversely, when aggregates were kept in a hyperoxic environment from day 12, corresponding to the photoreceptor differentiation onset, onward, an increased proliferation (Figures 2A–2BII and 2E) and a decreased amount of cell death (Figures 2C–2DII and 2F) were revealed at day 18 of culture. These results highlight the dual role exerted by hyperoxia on progenitor proliferation and photoreceptor survival during early and late stages of retinogenesis. However, aggregates maintained at atmospheric O_2 concentration up to day 25 reduced their GFP expression and retina size over time (Figure 2G). Consequently, hyperoxic conditions, applied from the time of photoreceptor differentiation onset onward, allowed the development of retinas with a volume increased up to five times over 10 days. Such protocol adjustments result in the formation of multilayered well-aligned GFP-positive retinas showing closer similarities to the in vivo development than the previous 3D protocol, as confirmed by the average number of GFP-positive cells (79% ± 1.8% versus 63% ± 2.2%) and photoreceptor rows (nine versus seven) produced per retina (Figure 3). Remarkably, the retina induction efficiency of the 3D culture system, measured as the number of aggregates containing at least one GFP-positive retina in comparison to the total number of aggregates, is around 79% ± 4.3% and 68% ± 3.5% using clones 3 and 6, respectively. Reliable induction of OC-OV was observed after a few passages, between 3 and 20, and between differentiation days 7 and 9, approximately one-third of the OVs underwent a quick morphological rearrangement, flattening,

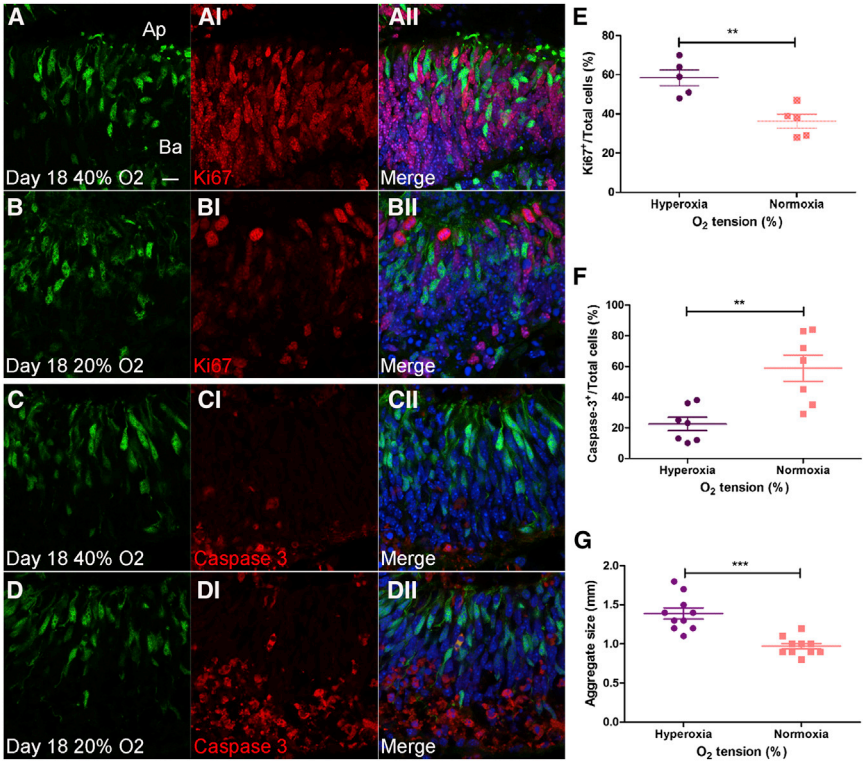

Figure 2. Hyperoxic Conditions to Increase Retina Size

OCs were incubated with normoxic or hyperoxic condition from day 12 onward.

(A–DII) Sections of retina-like tissues after 18 days of culture.

(A–AII and C–CII) Hyperoxic conditions (40% O_2).

(B–BII and D–DII) Atmospheric normoxia.

(E and F) Quantification of Ki67-positive (E) and caspase 3-positive (F) cells in normoxic and hyperoxic conditions.

(G) Quantification of the aggregate size at day 18 of culture in hyperoxia and normoxia.

All the figures presented have a correct apical-basal (Ap-Ba) polarization but with photoreceptors localized at the concave side of the retina as shown in (A).

**p < 0.01 and ***p < 0.001 by t test (n = 3 independent experiments with n = 3 biological replicates counted per experiment). Scale bar, 15 μm.

and consecutively invaginating their distal portion to give rise to OC-like structures.

In most of the cases when the invagination proceeded, round bright PAX6-positive structures resembling a primordial lens were observed in or near the OV invagination furrow (Figures S2A–S2D). At the end of the invagination process, lens-like structures were found to be displaced or had disappeared from the original position. At day 13 of culture, the first GFP-positive cells appeared inside either the OCs or the remaining OVs that had not invaginated. In fact, OVs unable to invaginate still demonstrated the capacity to produce photoreceptors resuming the canonical apical-basal polarization in an apical and concave shape, rather than convex, as highlighted by the laminin and N-cadherin expressions (Figures S2E–S2LI).

Time Course of the Photoreceptor Formation

At the end of the OC morphogenesis, the culture conditions established (see previous section) created an ideal and reproducible environment for the photoreceptor and retina development. Between days 12 and 14 of culture, GFP-positive cells arose in the most central part of the retina in a dispersed fashion similarly to what occurs in the neuroblastic layer of the developing E13 retina (Figures 4A–4BI and 4K–4KI). Between days 14 and 20, GFP-positive cells increased in number and progressively migrated toward the apical side of the retina to form a dense cell layer composed of numerous well-aligned photoreceptors (Figures 4C–4FI and 4L–4MI). At this time point, GFP-positive cells lined up to form photoreceptor rows equivalent to a postnatal day 0 (P0) retina in vivo. Between days 20 and 25, the retina size presented minor variations, and all the further modifications were mostly linked to the photoreceptor maturation (Figures 4E–4HI and 4M–4NI; see below, Retina and Photoreceptor Maturation). After 25–28 days of culture, a variable amount of retinas started developing rosettes (Figures 4I–4JI). In order to determine the peak time of photoreceptor birth in vitro, cell cultures were pulse labeled with 5-ethynyl-2′-deoxyuridine (EdU) for 24 hr or stained for Ki67 and analyzed for the GFP and EdU or Ki67 coexpressions. Photoreceptor birth was maximal between days 19 and 20 of culture (Figures S3A–S3D). It is noteworthy that aggregates at any differentiation stage were not completely synchronized in development, resulting in retinas with different sizes, shapes, and apical-basal orientation inside the aggregates. Nevertheless, a constant percentage of photoreceptors per retina, ranging between 73% and 85%, was revealed at the peak of the retinal size development (Figure 3).

Retina and Photoreceptor Maturation

After optimizing the protocol, we investigated whether the increase of photoreceptors affected the retinogenesis and whether the in vitro retina development paralleled the in vivo one. PAX6-positive (ganglion or amacrine cells;

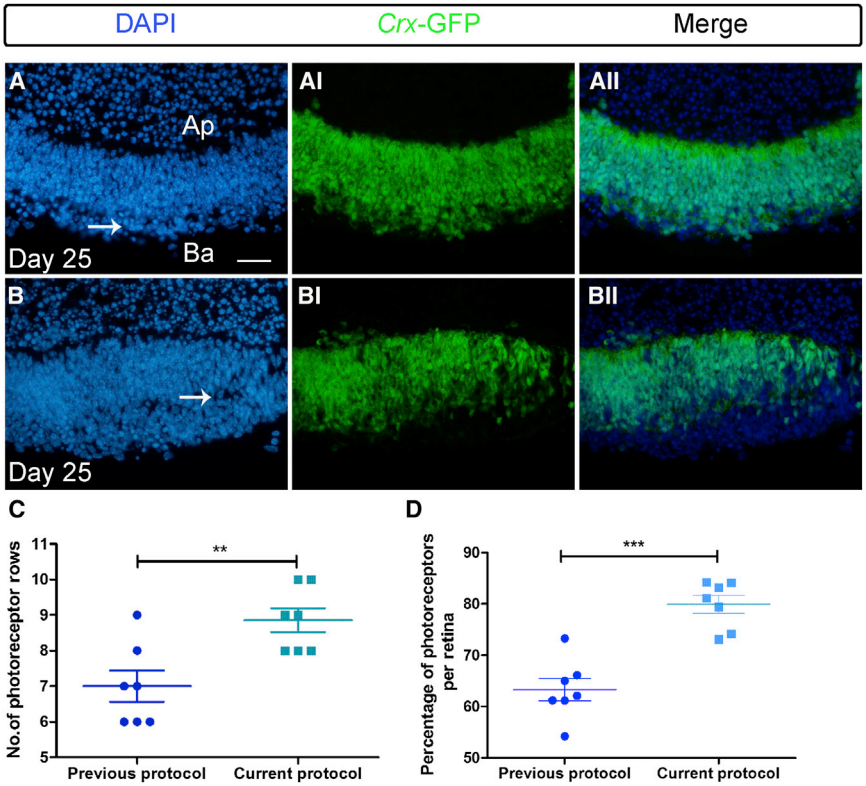

Figure 3. Comparison between the Number and Rows of Photoreceptors, per Retina, Obtained with the Present and the Former 3D Culture Protocol

(A–BII) Cryosections of day 25 retinas.

(A and B) Examples of complete (A) and incomplete (B) ONL/INL separation (white arrows).

(C and D) Quantification of photoreceptor rows (C) and photoreceptor number (D) obtained per retina.

The figures presented have a correct apical-basal (Ap-Ba) polarization with photoreceptors localized at the concave (A–AII) and at the convex (B–BII) side of the retina. The apical-basal polarization is shown in (A). DAPI nuclear stain is in blue. $^{**}p < 0.01$ and $^{***}p < 0.001$ by ANOVA with Tukey's correction (n = 7 independent experiments). Scale bar, 25 μm.

Figures S3E–S3EI), BRN3b-positive (ganglions; Figures S3F–S3FI), and RXRγ-positive cells (cones; Figures S3G–S3GI) were detected from day 13 onward. SOX9-positive retinal progenitors were present from day 13 up to days 20–22 of culture (Figures S3I–S3II). Sparse calbindin-positive cells (horizontal cells) with disoriented nuclei were identified from day 15 (data not shown). At this developmental stage, all the OTX2-positive cells were GFP positive, underlining the absence of bipolar cells (Figures S3H–S3HI). Two different populations of photoreceptor cells, the CRX-RXRγ-positive and CRX-positive-RXRγ-negative, were detected for the first time between days 13 and 15 of culture, confirming the presence of both cones and rods (Figures S3G–S3GI). The percentage of RXRγ-positive cells over the total GFP-positive photoreceptors was calculated. Of RXRγ-positive cones, 38% ± 1%, 27% ± 0.9%, 18% ± 1.1%, and 12% ± 1.2% were counted at days 16, 18, 20, and 23, respectively (Figure 5). The GFP expression perfectly parallels the in vivo development of the *Crx*-GFP mouse line (Samson et al., 2009) peaking in intensity at day 20. In this culture condition, the retinal-pigmented epithelium (RPE) differentiated from day 12 onward, but the structures analyzed showed development variations. In a few cases (3% ± 0.9%), the RPE completely enfolded the neural retina from the beginning, but most of the time, black-spotted cells patched the retina (Figure S4). In several experiments, the RPE differentiated in other locations, spreading along the surface of the aggregates. No obvious correlation was found between the RPE localization and the retina formation. From day 20, GFP-positive cells started producing sketches of the inner segments, and 5% ± 1.3% of them translated the cone phototransduction protein GNAT2 (Figures S5A–S5AI). At the same differentiation stage, OTX2-positive-GFP-negative cells (bipolar cells) were detected for the first time (Figures S5B–S5BI). Importantly, paralleling the in vivo development, Rhodopsin-positive photoreceptors were detected from day 20 onward (Figures S5C–S5CI). Other retinal cell types including PAX6-positive ganglion and amacrine cells as well as SOX9-positive retinal progenitors were still detected (Figures S5D–S5EI). After 25 days of culture, around 50% of the retinas began to separate the ONL from the inner nuclear layer (INL), even if the layer formation was often found to be incomplete (Figure 3, white arrows). The average diameter of the in-vitro-generated retinas peaked between days 23 and 25, to around 1.5 mm, fitting more with a P0 retina. From day 25 onward, structural synaptic proteins and functional components of the phototransduction cascade revealed by Ribeye, Bassoon, GNAT1, and GNAT2 were respectively detected (Figures S5F–S5II) with a pattern similar to that observed in P5 retinas. Other interneurons such as bipolar, amacrine, and ganglion cells

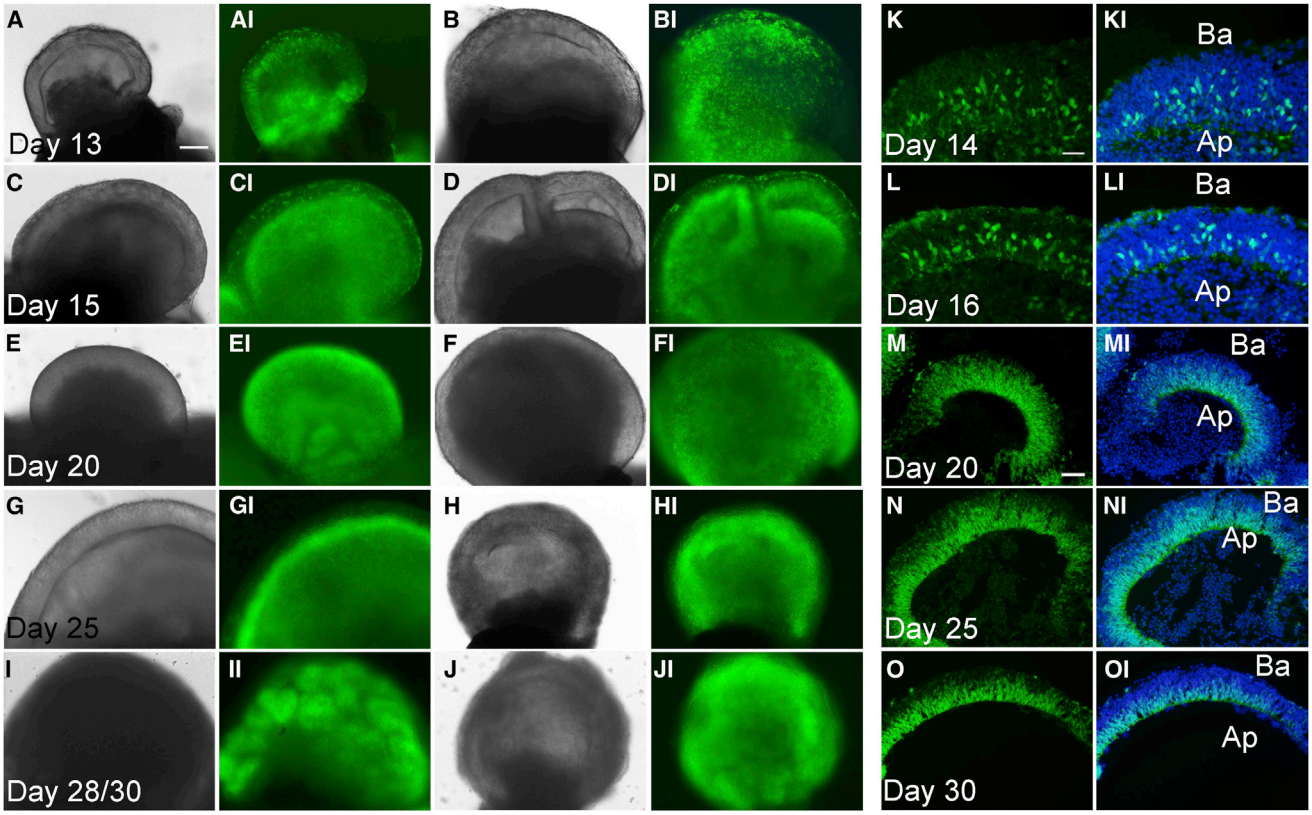

Figure 4. Time Course of Photoreceptor Formation from mESCs

(A–JI) Each differentiation stage is represented with two micrographs to highlight the heterogeneity of the in-vitro-generated retinas.
(A–BI) Appearance of GFP-positive photoreceptors.
(C–DI) Increase of photoreceptor number and alignment.
(E–FI) Peak of photoreceptor birth and GFP intensity.
(E–HI) Peak in retina size and in photoreceptor number.
(I–JI) Decrease in retinal size along with increase of rosette formation.
(K–OI) Micrographs of retina sections at various days of culture.
The figures presented have a correct apical-basal polarization but with photoreceptors localized at the concave (K–OI) side of the retina. The apical-basal polarization is shown in (KI), (LI), (MI), (NI), and (OI). DAPI nuclear stain is in blue.
Ba, basal side; Ap, apical side. Scale bars, 100 μm (A), 20 μm (K), and 50 μm (M).

were observed in all the retinas (Figures S5J–S5KI). Around 0.5% ± 0.2% of Vimentin-positive cells (Figures S5L–S5LI; Müller cells) were clearly distinguishable from day 25 onward.

In order to better determine the differentiation stage reached by the in-vitro-generated photoreceptors, the structure of the external segments was investigated. Centrin, expressed in the connecting cilium, basal body, and associated centrioles, and RPGRIP1L, found in the basal body, were utilized to identify the presence of the inner segments and the cilium of developing photoreceptors (Figures 6A–6C; RPGRIP1L not shown). Because the Centrin staining increases over time in evolving ciliary structures of developing photoreceptors, we determined that at day 25, the average size reached by the connecting cilium was similar to that of P4 photoreceptors (0.2–0.3 μm; Figures 6A–6C; Sedmak and Wolfrum, 2010). It is noteworthy that Centrin was revealed in photoreceptors either before dissociation or after fluorescence-activated cell sorting (FACS) procedures, even though sorted photoreceptors could be partially damaged (Figure 6D). ROM1 and Peripherin, two structural proteins involved in the morphogenesis and stabilization of the outer segments, localized at the distal tip of the connecting cilium before the outer segment formation, were not detected in retinas at differentiation days 25 and 30. The absence of such structural proteins highlighted the lack of the outer portion of the external segment, which during the in vivo development, is first detected in roughly 12% of P7 photoreceptors (Figure S6; Peripherin not shown). Based on the

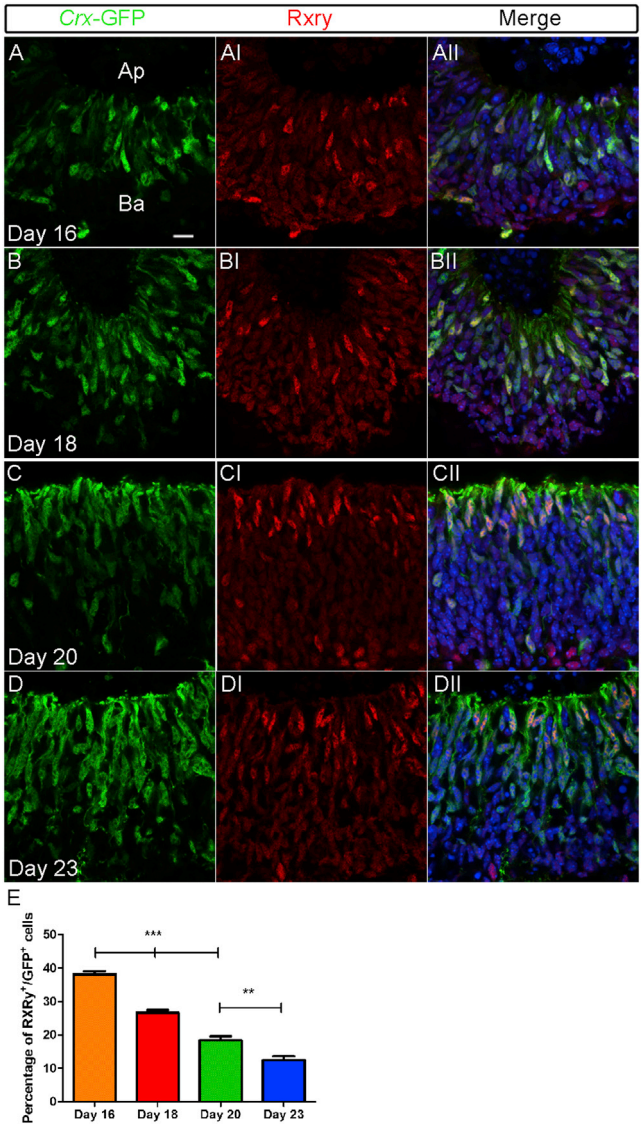

Figure 5. Percentage of Cones Generated from 3D Synthetic Retinas over Time

(A–DII) Cryosections of in-vitro-derived retinas at various differentiation stages.

(A–DII) GFP-positive photoreceptors in green.

(AI, BI, CI, and DI) RXRy-positive cones in red.

(AII, BII, CII, and DII) Merge with DAPI in blue.

(E) Quantification of RXRy-positive cells over total GFP-positive cells.

The figures presented have a correct apical-basal polarization with photoreceptors localized at the concave (A–BII and D–DII) and at the convex (C–CII) side of the retina. The apical-basal polarization is shown in (A).

**$p < 0.01$ and ***$p < 0.001$ by t test (n = 3 independent experiments with n = 3 technical replicates counted per experiment). Ba, basal side; Ap, apical side. Scale bar, 15 μm.

connecting cilium size, the absence of outer segment proteins, and together with the expression of functional photoreceptor proteins, retinas at day 25 of culture were equivalent to those at P4–P6 in vivo. Moreover, the translation of Bassoon and Ribeye, proteins responsible for the integrity of the ribbon complex of the synapses, highlights the capacity of such in-vitro-generated photoreceptors to make proper connections with the underlying bipolar cells showing a certain degree of maturation. At days 25–28, a variable amount of retinas started developing rosettes composed mostly of cells expressing simultaneous cone and rod markers (Opsin1, GNAT1, 2, and Rhodopsin; data not shown). Inversely, rosette-free retinas did not. After 28–30 days of culture, synthetic retinas decreased in size likely due to a massive apoptosis of different retinal cell types other than photoreceptors. No further morphological maturation of the external segments was observed up to day 45 of culture (data not shown).

Characterization of the Most Appropriate Stage to Transplant *Crx*-GFP-Positive Photoreceptors Generated with the 3D Culture System

The competence of ESC-derived photoreceptors to morphologically integrate adult retinas after transplantation was tested. Age-matched retina-like structures were pooled together and dissociated into a single-cell suspension (see Supplemental Experimental Procedures). GFP-positive photoreceptor cells were sorted by FACS. Around ten million photoreceptors were isolated per 96-well plate. The cells were then transplanted by subretinal injections into adult NOD/SCID recipient mice (see Experimental Procedures) to avoid the positive or negative influence that immune cytokines may have on photoreceptor survival and integration. In order to establish the most appropriate developmental stage for transplantation, photoreceptors were grafted at three differentiation time points (days 22, 25, and 30) and analyzed 3 weeks after transplantation. During this short period of time, sufficient to allow ESCs to develop tumors, none of the sorted and transplanted GFP-positive cells gave rise to tumor formation in the recipient mice. Integrated photoreceptors were well orientated within the ONL of the recipient retina (Figures 7A and 7B). A different integration competence was observed between photoreceptors collected at days 20, 25, and 30 of culture. Photoreceptors at day 25 showed the highest integration competence (around 799 ± 73 cells per retina; number of eyes injected [n] = 4; Figures 7A–7I), resembling more of those collected directly from P4 retinas (our internal control), known to be the best cell source for transplantation (MacLaren et al., 2006) (1,643 ± 137; n = 4 Figures 7I and S7). A lower capability to integrate recipient retinas was shown by older or younger in-vitro-derived

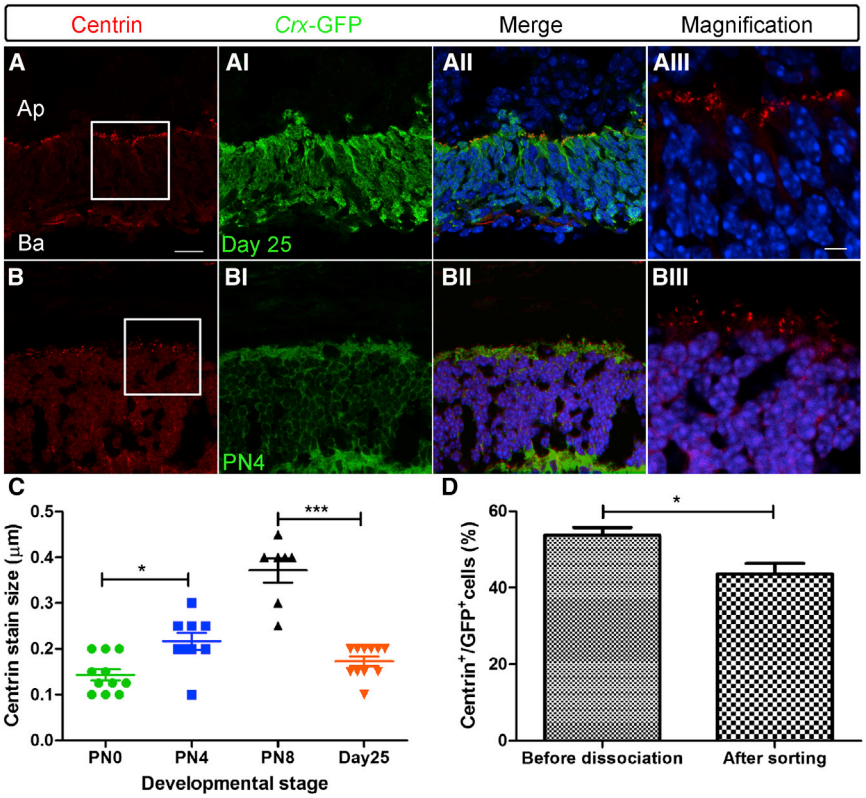

Figure 6. Centrin Expression in In-Vitro- versus In-Vivo-Developed Photoreceptors

Centrin stains the connecting cilium, basal body, and associated centriole.

(A–AIII) Centrin protein expressions (in red) at day 25 of culture and (B–BIII) in P4 retinas.

(AIII–BIII) Magnifications of (A and B) white-squared Centrin-positive cells merged with DAPI in blue.

(C) Quantification of Centrin size.

(D) Quantification of Centrin-GFP-positive photoreceptors before sorting on cryosectioned synthetic retinas and after sorting on floating cells at day 25 of culture. DAPI nuclear stain is in blue.

(A–BII) Correct apical-basal polarization with photoreceptors localized at the concave (A–AII) and at the convex (B–BII) side of the retina. The apical-basal polarization is shown in (A).

*$p < 0.05$ and ***$p < 0.001$ by ANOVA with Tukey's correction (n = 11 [P0], 9 [P4], 7 [P8], 11 [Day 25] independent experiments with n = 3 biological replicates counted per experiment). Ba, basal side; Ap, apical side. Scale bars, 20 µm (A) and 5 µm (AIII).

photoreceptors (656 ± 33 [n = 6] and 580 ± 32 [n = 7], respectively, cells per retina; Figure 7I). Importantly, unsorted cultured photoreceptors collected at any differentiation stage produced aggressive pigmented tumors after grafting in C57BL/6J mice (n = 5; data not shown). Moreover, unsorted photoreceptors dissected directly from P4 retinas did not give rise to tumors but produced only low integration success (n = 3; data not shown). All these results emphasized the need to isolate a pure population of photoreceptor cells before transplantation to maximize the photoreceptor integration and to increase the safety of the procedure. Finally, we assessed the morphological features displayed by mature integrated photoreceptors by immunocytochemistry. Integrated photoreceptors were positive for the outer segment marker ROM1, phototransduction pathway proteins GNAT1, PDE6b, and Rhodopsin (Figures 7C–7FI), and formed Bassoon- and Ribeye-positive active rod spherule synapses (Figures 7G and 7H), suggesting interaction within the recipient retina circuitry. Integrated rods show a correct apical-basal polarization and a directional light-mediated translocation of proteins such as Arrestin and GNAT1 (Figures 7J–7M).

It is noteworthy that mGluR6 and PKC-α proteins, localized postsynaptically at bipolar cell dendritic terminal tips and in rod bipolar cells, respectively, showed the capacity to extend dendrites toward the GFP-positive ribbon synapses of transplanted photoreceptors. Single-channel 3D images were analyzed for colocalization by Imaris and Just Another Colocalization Program (JACoP) plug-in on ImageJ (National Institutes of Health). Statistical data were reported from the Costes' randomization-based colocalization module. The colocalization analysis with GFP, PKC-α, and mGluR6 was performed in all three combinations. The statistical analyses provided, showing 100% colocalization between the fluorophores examined, strongly suggest a connection of the new synapses with the hosting bipolar cells (Figures 7N–7NIII and S7B–S7E).

In summary, in this work, we fine-tuned a 3D culture system enabling the production of large amounts of photoreceptors. A robust and reliable morphological integration of ESC-derived photoreceptors, along with the expression of key proteins present only in active ribbon synapses that colocalize with endogenous bipolar cells, was revealed after transplantation. In anticipation of the further characterization of the transplanted photoreceptors necessary to confirm their capacity to mediate light stimuli signals and restore visual functions, our results bring clear evidence laying the foundation for the use of in-vitro-derived photoreceptors to repair damaged retinas.

DISCUSSION

In this study, we provide a robust and reproducible protocol to obtain a large number of postmitotic, integration-competent photoreceptors, having adjusted a previously published protocol designed by Eiraku et al. (2011). The use of B27 supplement (Klassen et al., 2004; Merhi-Soussi et al., 2006; Djojosubroto and Arsenijevic, 2008; Giannelli et al., 2011) and the decrease of the FCS ratio from 10% to 1% allowed a reduction of extraocular tissue growth while favoring the development of a higher number of and better-aligned photoreceptor rows in comparison to those formed with the Eiraku protocol (seven to ten rows versus five to seven, respectively; Figure 3). The use of a higher concentration of O_2 (40% O_2) from day 12 rather than day 7, as previously published, provided a better environment to sustain the photoreceptor survival in vitro (Figure 2). All the ameliorations performed allowed a reproducible and robust production of retina-like tissues containing multilayered photoreceptor rows. From eight up to ten million *Crx*-GFP cells were routinely generated and simply harvested from a 96-multiwell plate. Notably, the hyperoxic conditions applied in the present 3D culture system are in contrast with a recently published work based on low-oxygen conditions to direct retinal progenitors toward photoreceptors from ESCs in 2D cultures (Garita-Hernández et al., 2013). The hypoxic conditions adopted allowed the induction of early retinal progenitors expressing RAX, SIX3, and PAX6, then giving rise to photoreceptors. Instead, in the present protocol, the use of hyperoxia was focused on sustaining photoreceptor survival once the cells are already formed (Figure 2). Even if in recognized literature the effects caused by different O_2 tensions are quite contrasting (Yu et al., 2004; Sirinyan et al., 2006; Wang and Linsenmeier, 2007; Bae et al., 2012), hyperoxic conditions have been demonstrated to increase photoreceptor oxygen consumption in avascularized retinas. Importantly, the in-vitro-derived retinas are not vascularized when photoreceptors develop the internal segment, which contains a high amount of mitochondria, responsible for the oxygen consumption of photoreceptors (Maslim et al., 1997). A hyperoxic condition, as tested in this work, thus seems to compensate for the vascularization deficit.

The advantage of this 3D culture system is the capacity of the induced retinal tissue to recapitulate precisely the in vivo development. At 25 days old, in-vitro-generated photoreceptors start expressing proteins involved in the phototransduction pathway such as GNAT1, and in the generation of active rod synapses such as Bassoon and Ribeye, thus resembling P4–P6 in-vivo-developed retinas. Moreover, the size of Centrin staining, expressed in the connecting cilium, basal body, and associated centrioles, confirms the similarity with the in vivo development. Indeed, the area of the Centrin staining increases over time, evolving in ciliary structures of developing photoreceptors (Sedmak and Wolfrum, 2010). Even if the ciliogenesis in rods is not completely synchronized, at day 25, the average size reached by the connecting cilium, highlighted by the Centrin antibody staining, was similar to that of P4 photoreceptors (0.2–0.25 versus 0.2–0.3 μm; Figure 6).

We then challenged the in-vitro-derived photoreceptors to integrate and mature inside the recipient retina. The use of a transgenic line prevents false-positive results as may occur in viral-transfected ESCs (West et al., 2012). Here, we transplanted ESC-derived photoreceptors at three differentiation stages, day 20, 25, or 30, into NOD-SCID mice retinas in order to evaluate the photoreceptor integration potential in the absence of inflammatory cytokines. The peak of photoreceptor integration was reached, as expected, by transplanting immature photoreceptors at day 25 of culture (Figure 7I). Indeed, based on the connecting cilium size, the phototransduction protein expression (GNAT1, Rhodopsin), the absence of ROM1 and Peripherin proteins (involved in the morphogenesis as well as the stabilization of the outer segments), and the transplantation study results, we can declare that retinas derived from ESCs at day 25 of culture are equivalent to those at P4–P6 in vivo. This morphological and cellular maturation corresponds to the stage of photoreceptor development with optimal competence to integrate a retina after transplantation (MacLaren et al., 2006). Morphologically integrated GFP-positive cells were well oriented and localized specifically in the ONL giving rise to the external segments and active ribbon synapses spanning the whole ONL thickness. Indeed, all integrated cells were GFP positive and translated the rod photosensitive pigment Rhodopsin, the structural protein of the external segment ROM1, the two phototransduction components GNAT1 and PDE6b, as well as the active rod synapse proteins Bassoon and Ribeye (Figure 7). Integrated rods show a directional light-mediated translocation of proteins such as Arrestin and GNAT1 (Figures 7J–7M). It is noteworthy that colocalization of the postsynaptic endogenous rod bipolar dendrites (PKC-α^+) and rod bipolar dendritic terminal tips (mGluR6$^+$), with the GFP-positive ribbon synapses of transplanted photoreceptors, was determined with a 100% statistical significance, suggesting the connection of the new synapses with the hosting bipolar cells (Figures 7N–7NIII and S7). These observations indicate a correct integration and maturation of the transplanted cells. In conclusion, this work demonstrates that the 3D culture system along with the use of the *Crx*-GFP ESC line allows the generation of in vitro retinas comprising integration-competent photoreceptors. Even if further characterization of the grafted photoreceptors is still needed to reveal their capacity to mediate light stimuli signals and restore visual functions,

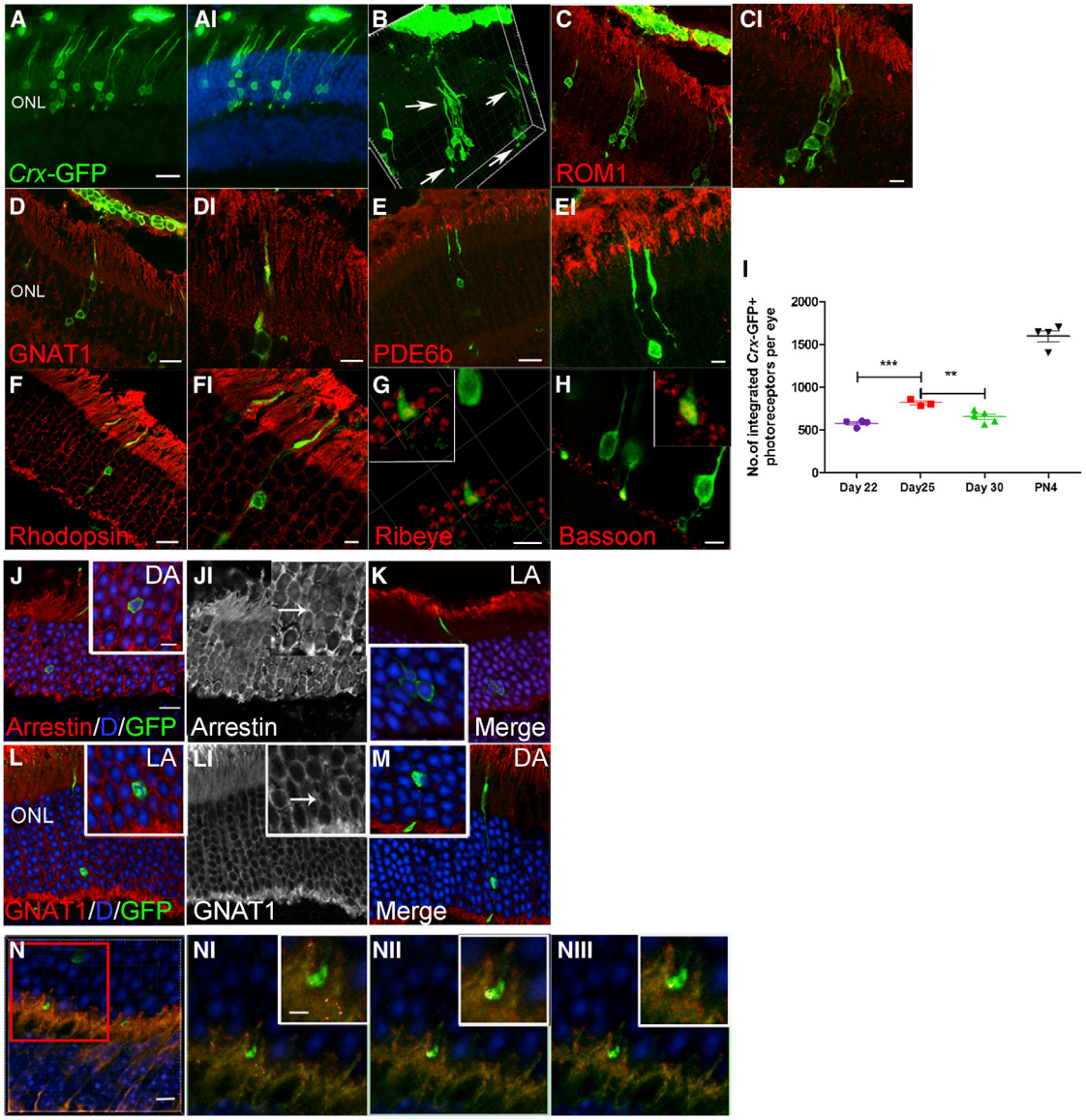

Figure 7. Transversal Sections of Adult NOD-SCID Mouse Retinas Transplanted with ESC-Derived Photoreceptors after 25 Days of Culture

(A–AI) Deconvolution pictures of morphologically integrated rod photoreceptors bearing the outer segment and spherule synapses (in green).

(B–H) Confocal images. (B) 3D reconstruction is shown of integrated rod bearing the external segment and spherule synapses (white arrows). Proteins involved in the phototransduction pathway such as ROM1 (C–CI), GNAT1 (D–DI), PDE6b (E–EI), and Rhodopsin (F–FI) are detected in the integrated cells. Synaptic ribbon proteins Ribeye (G) and Bassoon (H) are detected in the spherule synapses of the GFP-positive cells. The insets in (G) and (H) show the magnification of double-positive synapses.

(I) Quantification of morphologically integrated ESC-derived photoreceptors per injected eye, defined by the presence of the external segment or synapses. Number of injected eyes, n = 4 (Day 22), n = 3 (Day 25), n = 5 (Day 30), n = 4 (P4) with three technical experiment per eye.

(J–M) Opposite light-dependent distribution of rod Arrestin and GNAT1 in light- and dark-adapted retinas and transplanted photoreceptors.

(legend continued on next page)

our results give clear evidence of a morphological integration of in-vitro-derived photoreceptors. This work provides insight into how to achieve the production of photoreceptors compatible with transplantation requirements.

At the time of submission, Robin Ali's group published compelling results, transplanting ESC-derived photoreceptors differentiated from Eiraku's protocol as well (Gonzalez-Cordero et al., 2013). Although the photoreceptors generated by the two 3D culture systems were transplanted in different recipient mice, the former paper provides similar results concerning the transplantation efficiency: 0.3% versus 0.4% of the present protocol. The advantage of the *Crx*-GFP ESC line is the possibility to follow the photoreceptor genesis in vitro and determine the most appropriate differentiation stage for cell transplantation depending on cell maturation. Moreover, the present approach avoids the necessity of efficient viral-transfected photoreceptors that may be altered by the procedure and prevents the generation of false-positive results after grafting.

Importantly, this recent paper (Gonzalez-Cordero et al., 2013) together with our work confirms the capacity of pluripotent stem cells to provide a renewable source of cells to produce photoreceptors in vitro and highlights the great interest of using the 3D culture system developed by Sasai's group. Additionally, the use of the *Crx*-GFP ESC line in the culture conditions proposed in the present work brings a unique opportunity to follow the mammalian photoreceptor development in vitro. This paper provides insight into how to achieve production of photoreceptors compatible with transplantation requirements. It is now important to translate such knowledge to human pluripotent cells to reach a better comprehension of the mechanisms controlling the differentiation of future transplantation-competent human photoreceptors.

EXPERIMENTAL PROCEDURES

Animals

The mice used in this work were obtained from the Charles River Laboratories (C57BL/6J, NOD/SCID, and 129SvJ strains) or from The Jackson Laboratory (*Crx*-GFP line) and treated according to institutional and national as well as the Association for Research in Vision and in Ophthalmology guidelines. All the experiments as well as the procedures were approved by cantonal veterinary authorities. All mice were kept on the standard 12 hr dark-light cycle.

Blastocyst Recovery, Embryo Culture, ESC Line Isolation

Blastocysts were obtained from natural mating of 8-week-old *Crx*-GFP females (C57BL/6 background) crossed with 129SvJ male mice. For further details, see Supplemental Experimental Procedures.

Teratoma Assay

Immune-deficient 2-month-old NOD/SCID mice were injected subcutaneously using a 1 ml syringe with a bolus of 5×10^5 ESCs, inactivated mouse embryonic fibroblasts, and Matrigel (50% v/v in PBS). For further details, see Supplemental Experimental Procedures.

FACS Analysis

The in vitro retina-derived photoreceptors were dissociated according to the manufacturer's instructions using a Papain kit (Worthington Biochemical) and FACS sorted for GFP expression. Cell sorting was performed using a MoFlo Astrios (Beckman Coulter), fitted with a 488 nm green laser to excite GFP.

Transplantation of In Vitro Retina-Derived Photoreceptors

Adult recipient NOD/SCID mice were anesthetized with a reversible anesthetic regimen composed of ketamine/Dormitor (ketamine 30–60 mg/kg and Dormitor 0.5 –1 mg/kg) and reversed with the injection of Antisedan (0.5 –1 mg/kg). Recipient mice were transplanted between 6 and 12 weeks of age. For further details, see Supplemental Experimental Procedures. For the media used for cell isolation, propagation, differentiation, tissue/cell fixation, and immunohistochemistry/cytochemistry, as well as for PCR, RNA isolation, and reverse transcription, see Supplemental Experimental Procedures.

SUPPLEMENTAL INFORMATION

Supplemental Information includes Supplemental Experimental Procedures and seven figures and can be found with this article online at http://dx.doi.org/10.1016/j.stemcr.2014.04.010.

ACKNOWLEDGMENTS

We thank Professor Y. Sasai (Japan) for the *Rax*-GFP EB5 mESC line, Professor J. Sowden and R. Ali (UK) for their support, and Y.A. Barde for the J1 and R1 mESC lines. We warmly thank Rivolta's group (Lausanne) for providing cilium antibodies and for discussion on the work. We are also thankful for the technical assistance provided by the FACS facility at the Ludwig Cancer Research institute and at the CHUV in Lausanne and by two special technicians of our unit: Dana Wanner and Catherine Martin. We are grateful for the technical assistance of the confocal facility at the EPFL in

(N–NIII) Qualitative colocalization analysis of Manders' coefficient visualized on the images as white spots. (NI) mGluR6 versus PKC-α, (NII) GFP versus PKC-α, and (NIII) GFP versus mGluR6 channel are shown. DAPI nuclear stain is in blue.
**p < 0.01 and ***p < 0.001 by ANOVA with Tukey's correction. P4, postnatal day 4 retina-derived photoreceptors (n = 4); DA, dark adapted; LA, light adapted. Scale bars, 10 μm (A, D, E, and F), 4 μm (CI, DI, EI, FI, G, and H), 15 μm (J), 5 μm (inset in J), 5 μm (N), and 1 μm (inset in NI).

Lausanne. This work has been supported by the Novartis Foundation for medical-biological research, Provisu Foundation, Velux Foundation, and Fondation Asile des Aveugles.

Received: September 6, 2013
Revised: April 15, 2014
Accepted: April 16, 2014
Published: May 22, 2014

REFERENCES

Bae, D., Mondragon-Teran, P., Hernandez, D., Ruban, L., Mason, C., Bhattacharya, S.S., and Veraitch, F.S. (2012). Hypoxia enhances the generation of retinal progenitor cells from human induced pluripotent and embryonic stem cells. Stem Cells Dev. *21*, 1344–1355.

Bainbridge, J.W., Smith, A.J., Barker, S.S., Robbie, S., Henderson, R., Balaggan, K., Viswanathan, A., Holder, G.E., Stockman, A., Tyler, N., et al. (2008). Effect of gene therapy on visual function in Leber's congenital amaurosis. N. Engl. J. Med. *358*, 2231–2239.

Bemelmans, A.P., Kostic, C., Crippa, S.V., Hauswirth, W.W., Lem, J., Munier, F.L., Seeliger, M.W., Wenzel, A., and Arsenijevic, Y. (2006). Lentiviral gene transfer of RPE65 rescues survival and function of cones in a mouse model of Leber congenital amaurosis. PLoS Med. *3*, e347.

Bryja, V., Bonilla, S., and Arenas, E. (2006a). Derivation of mouse embryonic stem cells. Nat. Protoc. *1*, 2082–2087.

Bryja, V., Bonilla, S., Cajánek, L., Parish, C.L., Schwartz, C.M., Luo, Y., Rao, M.S., and Arenas, E. (2006b). An efficient method for the derivation of mouse embryonic stem cells. Stem Cells *24*, 844–849.

Busskamp, V., and Roska, B. (2011). Optogenetic approaches to restoring visual function in retinitis pigmentosa. Curr. Opin. Neurobiol. *21*, 942–946.

Cicero, S.A., Johnson, D., Reyntjens, S., Frase, S., Connell, S., Chow, L.M., Baker, S.J., Sorrentino, B.P., and Dyer, M.A. (2009). Cells previously identified as retinal stem cells are pigmented ciliary epithelial cells. Proc. Natl. Acad. Sci. USA *106*, 6685–6690.

Cideciyan, A.V., Jacobson, S.G., Beltran, W.A., Sumaroka, A., Swider, M., Iwabe, S., Roman, A.J., Olivares, M.B., Schwartz, S.B., Komáromy, A.M., et al. (2013). Human retinal gene therapy for Leber congenital amaurosis shows advancing retinal degeneration despite enduring visual improvement. Proc. Natl. Acad. Sci. USA *110*, E517–E525.

Decembrini, S., Cananzi, M., Gualdoni, S., Battersby, A., Allen, N., Pearson, R.A., Ali, R.R., De Coppi, P., and Sowden, J.C. (2011). Comparative analysis of the retinal potential of embryonic stem cells and amniotic fluid-derived stem cells. Stem Cells Dev. *20*, 851–863.

Djojosubroto, M.W., and Arsenijevic, Y. (2008). Retinal stem cells: promising candidates for retina transplantation. Cell Tissue Res. *331*, 347–357.

Eiraku, M., and Sasai, Y. (2012). Mouse embryonic stem cell culture for generation of three-dimensional retinal and cortical tissues. Nat. Protoc. *7*, 69–79.

Eiraku, M., Takata, N., Ishibashi, H., Kawada, M., Sakakura, E., Okuda, S., Sekiguchi, K., Adachi, T., and Sasai, Y. (2011). Self-organizing optic-cup morphogenesis in three-dimensional culture. Nature *472*, 51–56.

Garita-Hernández, M., Diaz-Corrales, F., Lukovic, D., González-Guede, I., Diez-Lloret, A., Valdés-Sánchez, M.L., Massalini, S., Erceg, S., and Bhattacharya, S.S. (2013). Hypoxia increases the yield of photoreceptors differentiating from mouse embryonic stem cells and improves the modeling of retinogenesis in vitro. Stem Cells *31*, 966–978.

Giannelli, S.G., Demontis, G.C., Pertile, G., Rama, P., and Broccoli, V. (2011). Adult human Müller glia cells are a highly efficient source of rod photoreceptors. Stem Cells *29*, 344–356.

Gonzalez-Cordero, A., West, E.L., Pearson, R.A., Duran, Y., Carvalho, L.S., Chu, C.J., Naeem, A., Blackford, S.J., Georgiadis, A., Lakowski, J., et al. (2013). Photoreceptor precursors derived from three-dimensional embryonic stem cell cultures integrate and mature within adult degenerate retina. Nat. Biotechnol. *31*, 741–747.

Gualdoni, S., Baron, M., Lakowski, J., Decembrini, S., Smith, A.J., Pearson, R.A., Ali, R.R., and Sowden, J.C. (2010). Adult ciliary epithelial cells, previously identified as retinal stem cells with potential for retinal repair, fail to differentiate into new rod photoreceptors. Stem Cells *28*, 1048–1059.

Gust, J., and Reh, T.A. (2011). Adult donor rod photoreceptors integrate into the mature mouse retina. Invest. Ophthalmol. Vis. Sci. *52*, 5266–5272.

Hirami, Y., Osakada, F., Takahashi, K., Okita, K., Yamanaka, S., Ikeda, H., Yoshimura, N., and Takahashi, M. (2009). Generation of retinal cells from mouse and human induced pluripotent stem cells. Neurosci. Lett. *458*, 126–131.

Kiyonari, H., Kaneko, M., Abe, S., and Aizawa, S. (2010). Three inhibitors of FGF receptor, ERK, and GSK3 establishes germline-competent embryonic stem cells of C57BL/6N mouse strain with high efficiency and stability. Genesis *48*, 317–327.

Klassen, H.J., Ng, T.F., Kurimoto, Y., Kirov, I., Shatos, M., Coffey, P., and Young, M.J. (2004). Multipotent retinal progenitors express developmental markers, differentiate into retinal neurons, and preserve light-mediated behavior. Invest. Ophthalmol. Vis. Sci. *45*, 4167–4173.

Lamba, D.A., Karl, M.O., Ware, C.B., and Reh, T.A. (2006). Efficient generation of retinal progenitor cells from human embryonic stem cells. Proc. Natl. Acad. Sci. USA *103*, 12769–12774.

Lamba, D.A., Gust, J., and Reh, T.A. (2009). Transplantation of human embryonic stem cell-derived photoreceptors restores some visual function in Crx-deficient mice. Cell Stem Cell *4*, 73–79.

Lamba, D.A., McUsic, A., Hirata, R.K., Wang, P.R., Russell, D., and Reh, T.A. (2010). Generation, purification and transplantation of photoreceptors derived from human induced pluripotent stem cells. PLoS One *5*, e8763.

MacLaren, R.E., Pearson, R.A., MacNeil, A., Douglas, R.H., Salt, T.E., Akimoto, M., Swaroop, A., Sowden, J.C., and Ali, R.R. (2006). Retinal repair by transplantation of photoreceptor precursors. Nature *444*, 203–207.

Maguire, A.M., Simonelli, F., Pierce, E.A., Pugh, E.N., Jr., Mingozzi, F., Bennicelli, J., Banfi, S., Marshall, K.A., Testa, F., Surace, E.M.,

et al. (2008). Safety and efficacy of gene transfer for Leber's congenital amaurosis. N. Engl. J. Med. *358*, 2240–2248.

Maslim, J., Valter, K., Egensperger, R., Holländer, H., and Stone, J. (1997). Tissue oxygen during a critical developmental period controls the death and survival of photoreceptors. Invest. Ophthalmol. Vis. Sci. *38*, 1667–1677.

Mathieson, K., Loudin, J., Goetz, G., Huie, P., Wang, L., Kamins, T.I., Galambos, L., Smith, R., Harris, J.S., Sher, A., and Palanker, D. (2012). Photovoltaic Retinal Prosthesis with High Pixel Density. Nat. Photonics *6*, 391–397.

Merhi-Soussi, F., Angénieux, B., Canola, K., Kostic, C., Tekaya, M., Hornfeld, D., and Arsenijevic, Y. (2006). High yield of cells committed to the photoreceptor fate from expanded mouse retinal stem cells. Stem Cells *24*, 2060–2070.

Meyer, J.S., Shearer, R.L., Capowski, E.E., Wright, L.S., Wallace, K.A., McMillan, E.L., Zhang, S.C., and Gamm, D.M. (2009). Modeling early retinal development with human embryonic and induced pluripotent stem cells. Proc. Natl. Acad. Sci. USA *106*, 16698–16703.

Nakano, T., Ando, S., Takata, N., Kawada, M., Muguruma, K., Sekiguchi, K., Saito, K., Yonemura, S., Eiraku, M., and Sasai, Y. (2012). Self-formation of optic cups and storable stratified neural retina from human ESCs. Cell Stem Cell *10*, 771–785.

Osakada, F., Ikeda, H., Mandai, M., Wataya, T., Watanabe, K., Yoshimura, N., Akaike, A., Sasai, Y., and Takahashi, M. (2008). Toward the generation of rod and cone photoreceptors from mouse, monkey and human embryonic stem cells. Nat. Biotechnol. *26*, 215–224.

Pearson, R.A., Barber, A.C., Rizzi, M., Hippert, C., Xue, T., West, E.L., Duran, Y., Smith, A.J., Chuang, J.Z., Azam, S.A., et al. (2012). Restoration of vision after transplantation of photoreceptors. Nature *485*, 99–103.

Prokofyeva, E., and Zrenner, E. (2012). Epidemiology of major eye diseases leading to blindness in Europe: a literature review. Ophthalmic Res. *47*, 171–188.

Samson, M., Emerson, M.M., and Cepko, C.L. (2009). Robust marking of photoreceptor cells and pinealocytes with several reporters under control of the Crx gene. Dev. Dyn. *238*, 3218–3225.

Sedmak, T., and Wolfrum, U. (2010). Intraflagellar transport molecules in ciliary and nonciliary cells of the retina. J. Cell Biol. *189*, 171–186.

Singh, M.S., Charbel Issa, P., Butler, R., Martin, C., Lipinski, D.M., Sekaran, S., Barnard, A.R., and MacLaren, R.E. (2013). Reversal of end-stage retinal degeneration and restoration of visual function by photoreceptor transplantation. Proc. Natl. Acad. Sci. USA *110*, 1101–1106.

Sirinyan, M., Sennlaub, F., Dorfman, A., Sapieha, P., Gobeil, F., Jr., Hardy, P., Lachapelle, P., and Chemtob, S. (2006). Hyperoxic exposure leads to nitrative stress and ensuing microvascular degeneration and diminished brain mass and function in the immature subject. Stroke *37*, 2807–2815.

Tomita, M., Adachi, Y., Yamada, H., Takahashi, K., Kiuchi, K., Oyaizu, H., Ikebukuro, K., Kaneda, H., Matsumura, M., and Ikehara, S. (2002). Bone marrow-derived stem cells can differentiate into retinal cells in injured rat retina. Stem Cells *20*, 279–283.

Tucker, B.A., Park, I.H., Qi, S.D., Klassen, H.J., Jiang, C., Yao, J., Redenti, S., Daley, G.Q., and Young, M.J. (2011). Transplantation of adult mouse iPS cell-derived photoreceptor precursors restores retinal structure and function in degenerative mice. PLoS One *6*, e18992.

Wang, S., and Linsenmeier, R.A. (2007). Hyperoxia improves oxygen consumption in the detached feline retina. Invest. Ophthalmol. Vis. Sci. *48*, 1335–1341.

West, E.L., Pearson, R.A., MacLaren, R.E., Sowden, J.C., and Ali, R.R. (2009). Cell transplantation strategies for retinal repair. Prog. Brain Res. *175*, 3–21.

West, E.L., Gonzalez-Cordero, A., Hippert, C., Osakada, F., Martinez-Barbera, J.P., Pearson, R.A., Sowden, J.C., Takahashi, M., and Ali, R.R. (2012). Defining the integration capacity of embryonic stem cell-derived photoreceptor precursors. Stem Cells *30*, 1424–1435.

Wray, J., Kalkan, T., and Smith, A.G. (2010). The ground state of pluripotency. Biochem. Soc. Trans. *38*, 1027–1032.

Wray, J., Kalkan, T., Gomez-Lopez, S., Eckardt, D., Cook, A., Kemler, R., and Smith, A. (2011). Inhibition of glycogen synthase kinase-3 alleviates Tcf3 repression of the pluripotency network and increases embryonic stem cell resistance to differentiation. Nat. Cell Biol. *13*, 838–845.

Yu, D.Y., Cringle, S., Valter, K., Walsh, N., Lee, D., and Stone, J. (2004). Photoreceptor death, trophic factor expression, retinal oxygen status, and photoreceptor function in the P23H rat. Invest. Ophthalmol. Vis. Sci. *45*, 2013–2019.

Zhang, J., Shan, Q., Ma, P., Jiang, Y., Chen, P., Wen, J., Zhou, Y., Qian, H., and Pei, X. (2004). Differentiation potential of bone marrow mesenchymal stem cells into retina in normal and laser-injured rat eye. Sci. China C Life Sci. *47*, 241–250.